The Journal of the Korean Society of Oceanography
Vol. 31, No. 2, pp. 75-88, June 1996

The Analytic and Numerical Solutions of the 1½-layer and 2½-layer Models to the Strong Offshore Winds.

HYONG SUN LEE
Korea Naval Academy, Chinhae City, Korea. 645-797

The analytic and numerical solution of the 1½-layer and 2½-layer models are derived. The large coastal-sea level drop and the fast westward speed of the anticyclonic gyre due to strong offshore winds using two ocean models are investigated. The models are forced by wind stress fields similar in structure to the intense mountain-pass jets(~20 dyne/cm^2) that appear in the Gulfs of Tehuantepec and Papagayo in the Central America for periods of 3~7 days. Analytic and numerical solutions compare favorably with observations, the large sea-level drop (~30 cm) at the coast and the fast westward propagation speeds (~13 km/day) of the gyres.

The coastal sea-level drop is enhanced by several factors: horizontal mixing, enhanced forcing, coastal geometry, and the existence of a second active layer in the 2½-layer model. Horizontal mixing enhances the sea-level drop because the coastal boundary layer is actually narrower with mixing.

The forcing τ/h is enhanced near the coast where h is thin. Especially, in analytic solutions to the 2½-layer model the presence of two baroclinic modes increases the sea-level drop to some degree. Of theses factors the strengthened forcing τ/h has the largest effect on the magnitude of the drop, and when all of them are included the resulting maximum drop is -30.0 cm, close to observed values.

To investigate the processes that influence the propagation speeds of anticyclonic gyre, several test wind-forced calculations were carried out. Solutions to dynamically simpler versions of the 1½-layer model show that the speed is increased both by β-induced self-advection and by larger h at the center of the gyres. Solutions to the 2½-layer model indicate that the lower-layer flow field advects the gyre westward and southward, significantly increasing their propagation speed.

The Papagayo gyre propagates westward at a speed of 12.8 km/day, close to observed speeds.

INTRODUCTION

The coastal-ocean response to the strong offshore winds in the Gulfs of Tehuantepec and Papagayo in the Central America has been stimulated by satellite observations (Stumpf and Legeckis, 1977). These observations and others reveal that the wind events force a large drop in coastal sea level, coastal upwelling, and the formation of an anticyclonic gyre that subsequently propagates westward and southward.

The strong offshore winds in the areas above are almost everywhere separated from the Pacific region by the mountainous topography of southern Mexico and Central America. However, air flows swiftly through three passes down the resulting pressure gradient, and forms narrow, intense jets in the Gulfs of Tehuantepec, Papagayo and Panama that blow almost directly offshore (Fig. 1). The wind jets off Tehuantepec are about 200 km wide, and extend abut 400 km offshore, and attain maximum wind stress values of the order of 20 *dyne/cm*^{2} (Roden, 1961).

In response to the strong offshore wind forcing, water moves rapidly offshore along the wind axis as it strengthens. Upwelling at the coast lowers coastal sea-level of the order of 30 cm, sea surface temperature (SST) drops by about 10°C, and entrainment cools SST farther offshore (Roden, 1961, Blackburn, 1962 and Alvarez *et al.*, 1989). Stumpf (1975), and Stumpf and Legeckis (1977) showed that an anticyclonic gyre develops on the western flank of the jet axis and propagates westward with a

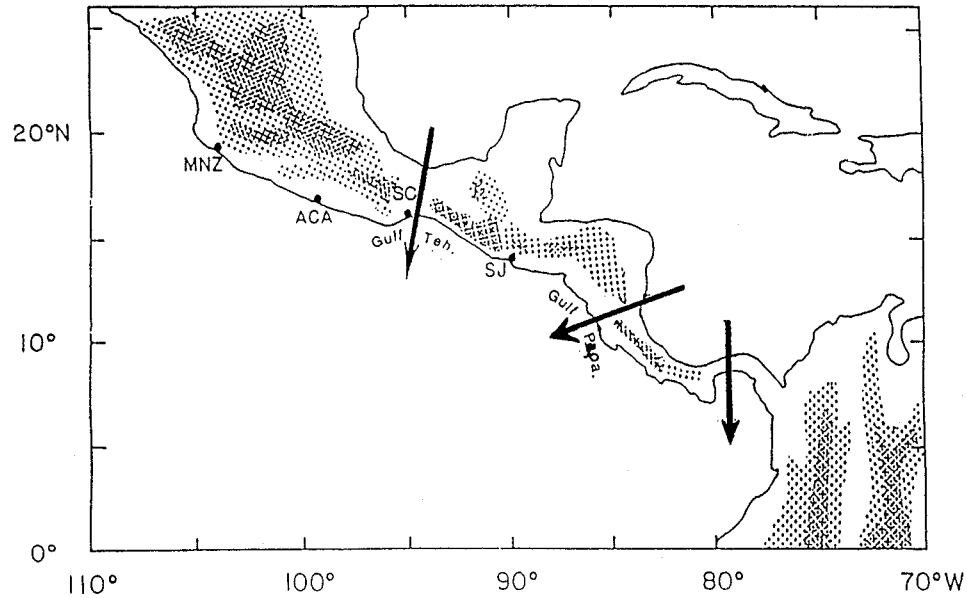

Fig. 1. A map showing the locations of the three mountain-pass jets. Light and dark shaded regions indicate where the elevation of the topography is greater than 650 and 2000 m, respectively. The locations of Manzanillo(MNS), Acapulco(ACA), Salina Cruz(SC) and San Jose(SJ) are indicated. The jets occur during the winter when high-pressure systems develop over the Gulf of Mexico. Air flows rapidly through the mountain passes down th pressure gradient. (after McCreary *et al*, 1989).

phase speed of about 15 cm/s (13 km/day).

Several theoretical studies have looked at the ocean's response to offshore winds. Millot and Crepon(1981), and Crepon and Richez(1982) found asymptotic analytic solutions to a linear two-layer model when the wind was directed perpendicular to the shore, constant in space, and a step function of time. They found that a coastal sea-level drop(d) and no Kelvin waves were generated by the wind, but did not describe the mechanism of d. Hua and Thomasset (1983) investigated the effects of coastline geometry on coastal upwelling using a two-layer, numerical model that allowed entrainment into the surface layer to occur whenever the bulk Richardson number was smaller than a critical value. They found that entrainment played an important role in determining the final shape of the upwelling centers in the nearshore region, but did not adequately simulate the development of the offshore gyre. Clarke (1988) studied the response in the Gulf of Tehuantepec using a simple 1½-layer model. He argued that the structure of a hypothesized inertial turning of the wind jet, was the primary cause of the anticyclonic eddy-like feature; however, according to Roden (1961), A. Trasvina *et al* (1995) and 1900-1979 COADS wind climatology for the months of November through February, there is little evidence for such a turning, with the wind extending 400-500 km directly offshore in the Gulf of Tehuantepec.

The observed gyres propagate offshore at speeds nearly twice the linear, non-dispersive Rossby wave speed $C_r = \beta g' H/f^2$ for a given parameters (Table 1) at 14.5 N, the predicted Rossby wave speed is only 3.5 *km/day*, much smaller than the observed speed of 7.5 *km/day*. Such a large propagation speed has not appeared in previous modelling studies of isolated eddies. McWilliams and Flierl (1979), and Nof(1981) demonstrated that in a quasi-geostrophic model C_r is the upper limit for the westward propagation speed of an isolated eddy. Matsuura and Yamagata(1982) showed that anticyclonic (cyclonic) gyres propagate westward at a speed slightly faster (slower) than C_r due to larger (smaller) layer thickness at the center of the gyre. Smith and Reid (1982) noted that isolated eddies in their 1½-layer prim-

itive-equation model all had propagation speeds less than C_r.

In this paper, the large sea level drop and fast westward speed of gyre are investigated using four ocean models: linear and nonlinear versions of each a $1\frac{1}{2}$-layer and a $2\frac{1}{2}$-layer model. The detail derivation of the solutions to the $1\frac{1}{2}$-layer model are shown in McCreary *et al* (1989).

THE MODEL OCEAN

Equations of Motion

a. The Linear $1\frac{1}{2}$-layer model: The linear $1\frac{1}{2}$-layer model has a single, active layer of density ρ_1 overlying a deep, inert layer of density ρ_2 where the pressure gradient is set to zero. Linearized equations of motion for the system are

$$\begin{aligned} &u_t - f\upsilon + p_x = \tau^x/H + \upsilon_h \nabla^2 u \\ &v_t + fu + p_y = \tau^y/H + \upsilon_h \nabla^2 \upsilon \\ &h_t + H(u_x + \upsilon_y) = 0, \end{aligned} \tag{1a}$$

and

$$p = g'(h - H) \tag{1b}$$

The continuity equation in (1a) can be replaced with

$$\frac{p_t}{c^2} + H(u_x + \upsilon_y) = 0, \tag{1c}$$

where $c^2 = g'H$. Common variables, u and υ are directed eastward and northward, respectively, the instantaneous thickness of the surface layer is h and its initial value is H, p is the pressure in the layer, f is the Coriolis parameter, υ_h is the coefficient of horizontal eddy viscosity, $g' = (\Delta\rho/\overline{\rho})g$ where $\Delta\rho = \rho_2 - \rho_1$, $\overline{\rho} = (\rho_2 + \rho_1)/2$, and g is the acceleration of gravity. The ocean can be forecd either by a meridional wind field τ^y or by a zonal wind field τ^x. Finally, sea level d is related to p and h by

$$d = p/g = (\Delta\rho/\overline{\rho})(h - H) \tag{2}$$

b. The Linear $2\frac{1}{2}$-layer model: The linear $2\frac{1}{2}$-layer model has a second active layer of density ρ_2 overlying a deep, inert layer of density ρ_3. Equations of motion are

$$\begin{aligned} &u_{it} - f\upsilon_i + p_{ix} = \delta_{i1}\tau^x/H_1 + \upsilon_h \nabla^2 u_i \\ &\upsilon_{it} + fu_i + p_{iy} = \delta_{i1}\tau^y/H_1 + \upsilon_h \nabla^2 \upsilon_i \\ &h_{it} + H_i(u_{ix} + \upsilon_{iy}) = 0, \end{aligned} \tag{3a}$$

and the p_i – fields in both layers are

$$\begin{aligned} p_1 &= g\varepsilon[\rho_{31}(h_1 - H_1) + \rho_{32}(h_2 - H_2)] \\ p_2 &= g\varepsilon[\rho_{32}(h_1 - H_1) + \rho_{32}(h_2 - H_2)]. \end{aligned} \tag{3b}$$

The subscript i in (3a) is a layer index (i = 1, 2), and common variables are defined the same as in equations (1). The quantity δ_{i1} is the Kronecker delta symbol, ε is the coefficient of thermal expansion (assumed constant), and density differences between layers are $\rho_{ij} = \rho_i - \rho_j$.

Equations (3a) can be summarized in the column – vector form,

$$\begin{aligned} &U_t - fV + P_x = \tau^x/H_1 + \upsilon_h \nabla^2 U \\ &V + fU + P_y = \tau^y/H_1 + \upsilon_h \nabla^2 V \\ &A \cdot P_t + U_x + V_y = 0, \end{aligned} \tag{4a}$$

where $\boldsymbol{q} = \begin{pmatrix} q_1 \\ q_2 \end{pmatrix}$ with q_i being u_i, v_i or p_i, $\tau^x = \begin{pmatrix} \tau^x \\ 0 \end{pmatrix}$, $\tau^y = \begin{pmatrix} \tau^y \\ 0 \end{pmatrix}$, and A is the martix

$$A = \begin{pmatrix} a_{11} & a_{12} \\ a_{21} & a_{22} \end{pmatrix} = \frac{1}{g\rho} \begin{pmatrix} 1/H_1 & -1/H_1 \\ -1/H_2 & \rho_{31}/(H_2\rho_{32}) \end{pmatrix} \tag{4b}$$

Solutions to (4a) can be represented as expansions in the two baroclinic (vertical normal) modes of the system,

$$q = \begin{pmatrix} q_1 \\ q_2 \end{pmatrix} = \tilde{q}_1\phi_1 + \tilde{q}_2\phi_2. \tag{5a}$$

where the modes ϕ_n are the eigenfunctions of matrix A

$$\phi_n = \begin{pmatrix} 1 \\ \lambda - a_{11})/a_{12} \end{pmatrix}, \tag{5b}$$

and are associated with the eigenvalues

$$\lambda_n = c_n^{-2} = \frac{1}{2}(a_{11}+a_{22}) + (-1)^n \frac{1}{2}[(a_{11}-a_{22})^2 + 4a_{12}a_{21}]^{\frac{1}{2}} . \quad (5c)$$

The equations of motion governing each mode are obtained by inserting (5a) into (4a) and taking the dot product of the eigenfunctions of the adjoint of A, $\hat{\phi}_n = [1,(\lambda_n - a_{11})/a_{21}]$. The result is

$$\begin{aligned} &\tilde{u}_{nt} - f\upsilon_n + p_{nx} = \tau^x/\mathcal{H}_n \\ &\tilde{u}_{nt} + f\tilde{u}_n + \tilde{p}_{ny} = \tau^y/\mathcal{H}_n \\ &\tilde{p}_{nt}/c_n^2 + \tilde{u}_{nx} + \upsilon_{ny} = 0 \end{aligned} \quad (6)$$

where $\mathcal{H}_n = H_1[1+(\lambda_n - a_{11})^2/a_{12}a_{21}]$. Note that equations (6) are identical in form to equations (1c) for the 1½-layer model, differing only in the values for c_n^2 and $\mathcal{H}_n$.

With the aid of (5a) and (5c), sea level can also be expressed as

$$d = p_1/g = \tilde{d}_1 + \tilde{d}_2 = (\tilde{p}_1 + \tilde{p}_2)/g, \quad (7)$$

so that the total sea-level drop is just sum of each drop associated with each mode.

c. The nonlinear 1½-layer model: Equations of motion for this system are

$$\begin{aligned} &(hu)_t + (uhu)_x + (\upsilon hu)_y - fh\upsilon + hp_x = \tau^x + \upsilon_h \nabla^2(hu) \\ &(h\upsilon)_t + (uh\upsilon)_x + (\upsilon h\upsilon)_y + fhu + hp_y \\ &\quad = \tau^y + \upsilon_h \nabla^2(h\upsilon) \quad (8a) \\ &h_t + (hu)_x + (h\upsilon)_y = \omega_e \\ &T_t + uT_x + \upsilon T_y = Q/h - \omega_e(T - T_e)/h + k_h \nabla^2 T, \end{aligned}$$

and the pressure gradient is

$$\nabla p = \varepsilon g \nabla[h(T - T_d)] - \frac{1}{2}\varepsilon g h \nabla T. \quad (8b)$$

Common variables are defined the same as in (1). Note that, because the surface temperature T is not constant in this thermodynamic model, ∇p includes the extra term-½ $\varepsilon g h \nabla T$. Additional quantities are T_a and T_e, the temperatures of the deep ocean and the water entrained into the surface layer, respectively. Strictly speaking, T_e must equal T_a in the nonlinear 1½-layer model. Three thermodynamic processes affect T: the heat flux Q through the ocean surface, horizontal diffusion of heat with coefficient k_h, and entrainment described by the velocity w_e. Sea level is given by

$$d = \varepsilon[h(T - T_d) - H(T_o - T_d)], \quad (9)$$

where T_o is the initial value of T. Due to the nonlinear dependence of d on h and T, sea level can

Table 1. Parametes for all the ocean models used in this paper unless specified otherwise. All the values are chosen as reallistically as possible for the Gulf of Tehuantepec

Parameter	Notation	Value
Initial upper-layer thickness	H_1	50 m
Initial lower-layer thickness	H_2	250 m
Mode-1 characteristic thickness	$\mathcal{H}_1$	201.5 m
Mode-2 characteristic thickness	$\mathcal{H}_2$	66.5 m
Entrainment thickness	H_e	50 m
Initial upper-layer temperature	T_o	29°C
Deep-layer temperature, 1½-layer model	T_a	12°C
Second-layer temperature, 2½-layer model	T_2	12°C
Deed-layer temperature, 2½-layer model	T_3	0°C
Coefficient of thermal expansion	ε	3×10^{-4} C^{-1}
Thermodynamic time constant	t_e	0.125 day
Heating time constant	t_h	50 day
Horizontal mixing coefficients	υ_h, k_h	2×10^7 cm^2/s
Coriolis parameter at 16°N	f	$4\times10^{-5}s^{-1}$
Coriolis parameter at 11°N	f	$2.77\times10^{-5}s^{-1}$
Acceleration of gravity	g	980 cm^2/s
Reduced-gravity acceleration	g'	5 cm^2/s
Characteristic speed, 1½-layer model	c	158 cm/s
Mode-1 characteristic speed	c_1	33.2 cm/s
Mode-2 characteristic speed	c_2	140.7 cm/s

only drop to a minimum value of $-\varepsilon H(T_o - T_d)$, which for the given parameters in Table 1 is -25.5 cm. A similar limit does not exist in the linear models since T does not change, nor does it exist for the nonlinear 2½-layer model discussed next.

The surface heat flux(Q) and entrinment (w_e) are given by as in McCreary *et al* (1989)

$$Q = \frac{H}{t_h}(T_o - T) \tag{10}$$

and

$$w_e = \begin{cases} (H_e - h)^2/(t_e H_e) & h < He \\ 0 & otherwise. \end{cases} \tag{11}$$

According to (10) and (11), t_h is a measure of the e – folding time for the upper – layer temperature to relax back to T_o. Entrainment exists only when h is less than a specified value H_e and increases parabolically toward a maximum value of H_e/t_e as h goes to zero. The entrainment time scale t_e must be small enough to ensure that the interface does not surface in intense upwelling regions, otherwise solutions are not particularly sensitive to its value.

d. The nonlinear 2½-layer model: This model has two active layers, as used by McCreary and Kundu (1988). Equations of motion in the upper – layer, denoted by 1, are

$$\begin{aligned}
&(h_1u_1)_t + (u_1h_1u_1)_x + (v_1h_1u_1)_y - fh_1v_1 \\
&\quad + h_1p_{1x} = \tau^x + \omega_e u_2 + v_h\nabla^2(h_1u_1) \\
&(h_1v_1)_t + (u_1h_1v_1)_x + (v_1h_1v_1)_y + fh_1u_1 \\
&\quad + h_1p_{1y} = \tau^y + \omega_e v_2 + v_h\nabla^2(h_2v_2) \qquad (12a) \\
&h_{1t} + (h_1u_1)_x + (h_1v_1)_y = \omega_e \\
&T_{1t} + u_1T_{1x} + v_1T_{1y} = Q/h_1 - \omega_e(T_1 - T_e)/h_1 + k_h\nabla^2T_1,
\end{aligned}$$

and the lower layer equations, denoted by 2, are

$$\begin{aligned}
&(h_2u_2)_t + (u_2h_2u_2)_x + (v_2h_2u_2)_y - fh_2v_2 + h_2p_{2x} \\
&\quad = -\omega_e u_2 + v_h\nabla^2(h_2u_2) \\
&(h_2v_2)_t + (u_2h_2v_2)_x + (v_2h_2v_2)_y + fh_2u_2 + h_2p_{2y} \\
&\quad = -\omega_e v_2 + v_h\nabla^2(h_2v_2) \\
&h_{2t} + (h_2u_2)_x + (h_2v_2)_y = -\omega_e \qquad 12b) \\
&T_{2t} = 0.
\end{aligned}$$

Pressure gradients in the two layers are given by

$$\begin{aligned}
\nabla p_1 &= \varepsilon g\nabla[h_1(T_1 - T_3) + h_2(T_2 - T_3)] - \frac{1}{2}\varepsilon g h_1\nabla T_1, \\
\nabla p_2 &= \varepsilon g(T_2 - T_3)\nabla(h_1 + h_2),
\end{aligned} \tag{12c}$$

and sea level d is

$$\begin{aligned}
d = \varepsilon[h_1(T_1 - T_3) + h_2(T_2 - T_3)] - \varepsilon[H_1(T_o - T_3) \\
+ H_2(T_2 - T_3)],
\end{aligned} \tag{13}$$

where T_3 is the temperature of the deep ocean. Note that the sea-level drop is not as severely limited as for the nonlinear 1½-layer model because of the additional dependence on h_2.

Schemes and Parameters

Analytic and numerical schemes are the same as those in McCreary *et al* (1989). The details must be referred in their schemes. The numerical scheme of the nonlinear models integrate the temperature equation for the upper-layer temperature field. Analytic solutions are found in either an unbounded basin or a semi-infinite basin at y = 0. For the numerical solutions assuming a rectangular basin, boundary conditions on the northern, eastern and southern boundaries are the no – slip conditions,

$$u_i = v_i = 0, \quad T_{in} = 0, \quad h_{in} = 0 \tag{14a}$$

where as on the western boundary they are the open conditions

$$u_{in} = v_{in} = 0, \quad T_{in} = 0, \quad h_{in} = 0 \tag{14b}$$

where the subscripts i and n are a layer index (i = 1, 2), and a partial derivative in a direction normal to the boundary, respectively.

The grid dimensions are $\Delta x = \Delta y = 20$ km, and the time step is $\Delta t = 30$ min, some calculations are also carried out on a finer grid with $\Delta x = \Delta y = 5$ km and $\Delta t = 6$ min. The choice of time step is chosen to be just small enough to satisfy the CFL condition:

$$\Delta t \le \Delta x/(2\sqrt{2}c).$$

The model oceans are forced by wind fields similar in strength and structure to the Tehuantepec and

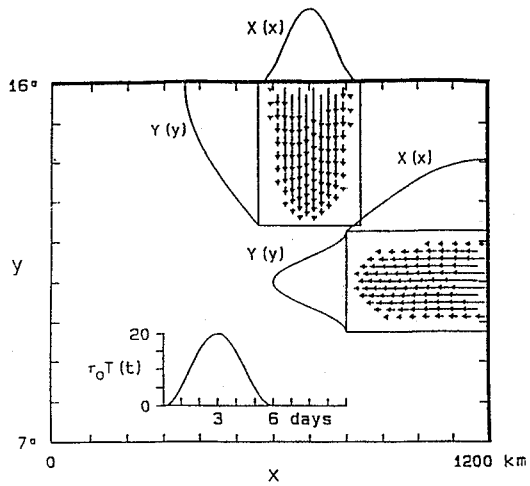

Fig. 2. A schematic diagram illustrating the spatial and temporal structures of the wind fields forcing the Tehuantepec and Papagayo solutions. Both jets are directed off-shore, are 280 km wide and 400 km long, and the absolute value of the maximum stress is 20 *dyne/cm*^{2} (after McCreary *et al*, 1989).

Papagayo jets. They have the separable form

$$\tau = \tau_0 X(x) Y(y) \mathcal{T}(t) \tag{15}$$

where τ is always directed offshore.

Figure 2 illustrates the wind fields that force all the numerical solutions, The figure shows the locations of the wind fields, as well as their spatial and temporal structures, X(x), Y(y) and $\mathcal{T}(t)$. For the Tehuantepec wind, the zonal structure is

$$X(x) = \begin{cases} \frac{1}{2}[1+\cos\frac{2\pi(x-x_m)}{x_\omega}] & |x-x_m| < x_\omega/2 \\ 0 & \textit{otherwise.} \end{cases} \tag{16}$$

where $x_m = 700$ km and $x_\omega = 280$ km, and meridional structure is

$$Y(y) = \begin{cases} \cos\frac{2(y-y_m)}{2y_\omega} & y > y_m - y_\omega \\ 0 & \textit{otherwise} \end{cases} \tag{17}$$

where $y_m = 16$ N and $y_\omega = 400$ km. For the Papagayo wind, the structures are similarly defined, with x and y interchanged and with $x_m = 1200$ km and $y_m = 11$ N. The time dependence of the wind, defined by

$$\mathcal{T}(t) = \begin{cases} \frac{1}{2}[1-\cos 2\pi\frac{t}{t_\omega}] & t < t_\omega \\ 0 & \textit{otherwise.} \end{cases} \tag{18}$$

with $t_\omega = 6$ days, The strength of the wind is $\tau_0 = -20$ dyne/cm^2.

Parameters for the ocean models are set to values that are as realistic as possible and listed in Table 1. For most of the solutions $T_d = T_2$; properties of solutions with $T_d = T_3$ are discussed in Section 3. The temperature of the water entrained into the surface layer is always T_2. The Coriolis parameter f is either constant or given by $f = 2\,\Omega\sin(y/R_e)$, where $\Omega = 2\pi/day$ and $R_e = 6370$ km is the radius of the earth. When f is constant, it has the value $f = 4.0\times10^{-5}$ s^{-1} for the Tehuantepec case and $f = 2.77\times10^{-5}$ s^{-1} for the Papagayo case.

WIND – FORCED SOLUTIONS

Solutions to the 1½-layer Model

a. Analytic solutions: In this Section, analytic solutions are found on the *f*-plane in 3 different situations: for a spatially uniform, switched – on wind in semi – infinite ocean, for a spatially bounded wind patch without horizontal mixing, and for a wind periodic in *x* and t with horizontal mixing. In order to illustrate as clearly as possible the important physical processes, solutions are arranged in a hierarchy of increasing dynamical complexity. Derivations and discussions of the first two solutions must be referred in McCreary *et al* (1989).

i. Uniform meridional wind, semi-infinite basin: With a northern boundary at y = 0, the forcing has the form $\tau^y = \tau_0\mathcal{T}(t)$, f is constant, and the solution is

$$u = \frac{\tau_0}{f}H(1-e^{\alpha y})\mathcal{T}, v = \frac{\tau_0}{fH}(1-e^{\alpha y})\mathcal{T}, p = c\frac{\tau_0}{fH}e^{\alpha y}\mathcal{T} \tag{19}$$

where $\alpha = f/c$ is the reciprocal of the Rossby radius of deformation. According to (19) and (2), sea level

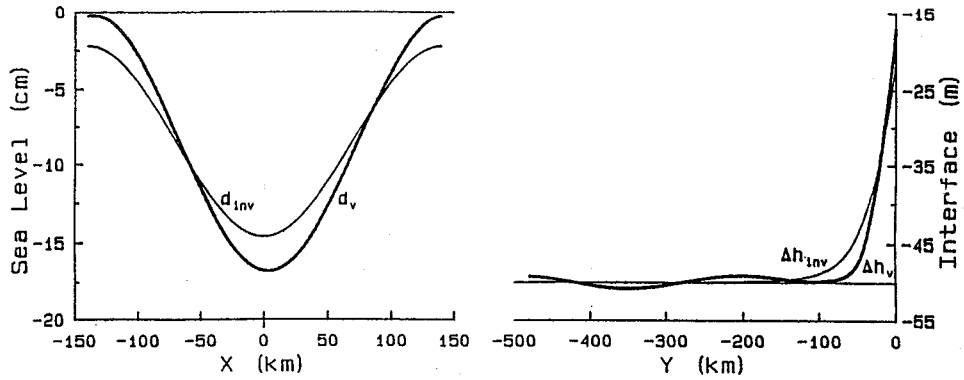

Fig. 3. Coastal(y = 0)sea-level drop at day 3 with mixing d_v and without mixing d_{inv} (left panel), showing maximum drops of -16.8 cm and -14.5 cm, respectively. The interface structures Δh_v and Δh_{inv}, along the wind axis (x = 0) at day 3 (right panel), showing that the decaying structure with mixing is more narrower, and so steeper.

at the coast is $d = p/g = -16.1\,cm$ (at 3 days) for the given parameter.

ii. Wind patch, semi-infinite basin: For this solution, the forcing has the spatially limited form (16 and 17) and f is constant. With the assumptions that the wind is slowly varying in time and large scale space, the solution is

$$u = \frac{\tau_0}{fH}X[Y - Y(0)e^{ay}]\mathcal{T} + \frac{c^2\tau_0}{f^2H}X_x[Y_y - aY(0)e^{ay}] \int_0^t \mathcal{T}(\mathrm{r})\,\mathrm{dr}$$

$$v = \frac{\tau_0}{f^2H}X[Y - Y(0)e^{ay}]\mathcal{T}t - \frac{c^2\tau_0}{f^2H}X_{xx}[Y - Y(0)e^{ay}] \int_0^t \mathcal{T}(\mathrm{r})\,\mathrm{dr} \qquad (20)$$

$$p = \frac{c\,\tau_0}{fH}XY(0)e^{ay}\mathcal{T} - \frac{c^2\tau_0}{f^2H}HY_y\mathcal{T} - \frac{c^2\tau_0}{f^2H}X_x[Y - Y(0)e^{ay}] \int_0^t \mathcal{T}(\mathrm{r})\,\mathrm{dr}$$

Equation (20) clearly shows the direct counterparts of those in solution (19) and the Ekman pumping terms. The second terms of u and v describe two counter-rotating gyres. The largest drop in coastal sea level is -14.1 cm (at 3 days). There are no coastal Kelvin waves in (20)

iii. Wind periodic in x and t, semi – infinite basin, horizontal mixing: For the analytic solutions to equations (1) with horizontal mixing, we simplify the forcing to be independent of y and periodic in space and time by choosing the functions in (16-18) to be

$$\mathrm{Y(y)} = 1,\ \mathcal{T}(\mathrm{t}) = -\cos\,\sigma t \text{ and } X(x) = \frac{1}{2}(1 + \cos kx)$$

where $\sigma = 2\pi/t_\omega$ and $k = 2\pi/x_\omega$

Then, the forcing is

$$\tau^y = -(\tau_0/2)(1 + \cos kx)\cos\sigma t.$$

The solution is straight forward but algebraically lengthy, and so the derivation is not shown here and must be referred in Lee (1990). According to his equations (B18) and (B21), the coastal sea-level response at y=0 is

$$d = d_\omega + d_e + d_s = a_\omega\cos(kx + \sigma t + \Phi_\omega) + a_e\cos(-kx + \sigma t + \Phi_e) + a_s\cos(\sigma t + \Phi_s), \qquad (21a)$$

where a and Φ are amplitude and phases(Table 2), respectively. Then, along the wind axis at x = 0 is

$$d(x=0) = a_1e^{l11y}\cos(-l_{12}y + \sigma t + \Phi_1) + a_2e^{l21y}\cos(l_{22}y + \sigma t + \Phi_2) + a_3e^{l11y}\cos(-l_{12}y + \sigma t + \Phi_3) + a_4e^{l21y}\cos(l_{22}y + \sigma t + \Phi_4) + a_5e^{l'11y}\cos(-l'_{12}y + \sigma t + \Phi_5) + a_6e^{l'21y}\cos(l'_{22}y + \sigma t + \Phi_6). \qquad (21b)$$

Table 2. Amplitudes (cm) and phases (radian) of sea level shown in equations (22)

Amplitude	Phases
a_0=6.95	Φ_0=0.0294
a_1=13.42	Φ_1=-0.4076
a_2=4.22	Φ_2=1.8052
a_3=5.13	Φ_3=2.6778
a_4=3.59	Φ_4=-1.1430
a_5=8.30	Φ_5=-0.0524
a_6=0.26	Φ_6=0.4296
a_w=4.61	Φ_w=-0.3131
a_e=3.93	Φ_e=-0.1972
a_s=8.53	Φ_s=-0.3131

Figure 3 contrasts the viscid and inviscid versions of these solutions at day 3, showing coastal sea level in the left panel and upper-layer thickness ($\Delta H = h - H = \bar{d}\rho/\rho_{12}$) along the wind axis in the right panel. Because the phase angles in (21a) are not zero (see Table 2), the minimum coastal sea level occurs neither at day 3 nor at the wind axis; instead, the minimum value of -17.0 cm actually occurs at 3.14 days (a 3.4 hour lag) and at x=3 km. This sea-level drop is 16% larger than that(-14.6 cm at x=0 and t=3 days) of the corresponding inviscid solution. Thus, horizontal mixing acts to shift the location and time of minimum sea level slightly, but to increase the sea-level drop much larger.

It is surprising that the sea-level drop is increased by horizontal mixing. A possible reason for this increase is that the volume of water displaced offshore by the forcing is greater with mixing than without it. To test this idea we determined the average offshore transport per wavelength, V, driven by the forcing as it increased from zero(at $t=\pi/\sigma$=3 days) to its maximum strength (at $f = 2\pi/\sigma = 6$ days). It is sufficient to evaluate this transport far offshore where the offshore velocity is just v' and the result is

$$V = \rho\frac{H}{x_\omega}\int_{-x_\omega/2}^{x_\omega/2} dx \int_{\pi/2\sigma}^{\pi/\sigma} dt\, v' = \frac{-\rho\tau_o}{2(f^2-\sigma^2)}, \qquad (22)$$

which is the same both with and without mixing. The other possibility for the increased sea-level drop is that mixing changes the structure of the coastal boundary layer, and this is indeed the case. The plots in the right panel of Figure 3 show that the boundary layer with mixing is actually narrower than that without mixing. Thus, to provide a volume of water equal to the amount that is displaced offshore, the interface in the narrower boundary layer must rise further (and hence the sea-level drop must increase).

b. Numerical solutions:

For the linear model to the Tehuantepec forcing when f is costant, coastal sea level has dropped -18.7 cm, at day 3 which is 33% more than the drop of -14.1 cm associated with the inviscid analytic solution, due to horizontal mixing in the numerical model.

For the papagayo forcing, the variable f solution shows that the speed of the gyre is only 3.8 km/day, considerably smaller than the nondispersive Rossby wave speed at 12°N of 5.3 km/day. For Tehuantepec solution when f is variable, the sea level drops -25.0 cm at the coast after 3 days, considerably larger than the value of -18.7 cm for the linear model.

To determime the causes of the increase in the sea-level drop from -18.7 cm to -25.0 cm, we carried out a series of test calculations in which various terms were sequentially neglected or linearized in the momentum and continuity equations in (8a). When the forcing term was then linearized the drop decreased markedly to -12.0 cm and for the completely linearized model it was -18.5 cm, in good agreement with the solution to the linear model. Clearly, the most important term causing the increase is the forcing τ/h, where the shallowing of h at the coast during upwelling.

For the Ppagayo forcing, the westward speed of the gyre is 6.3 km/day, much faster than that of the linear solution not shown here. The increased propagation speed probably has two nonlinear cause: the momentum-advection term, and the nonlinear terms with the larger layer thikness at the center of the gyre.

In all the previous solutions, the propagation speeds of anticyclonic gyres are considerably less than those of observed ones. A possible reason for this discrepancy is that the background stratification is not well represented,and therefore that the speeds of free waves are underestimated. To explore the sensitivity of solutions to the background stratification, we carried out several runs that were the same as the Tehuantepec and Papagayo solutions in Figures

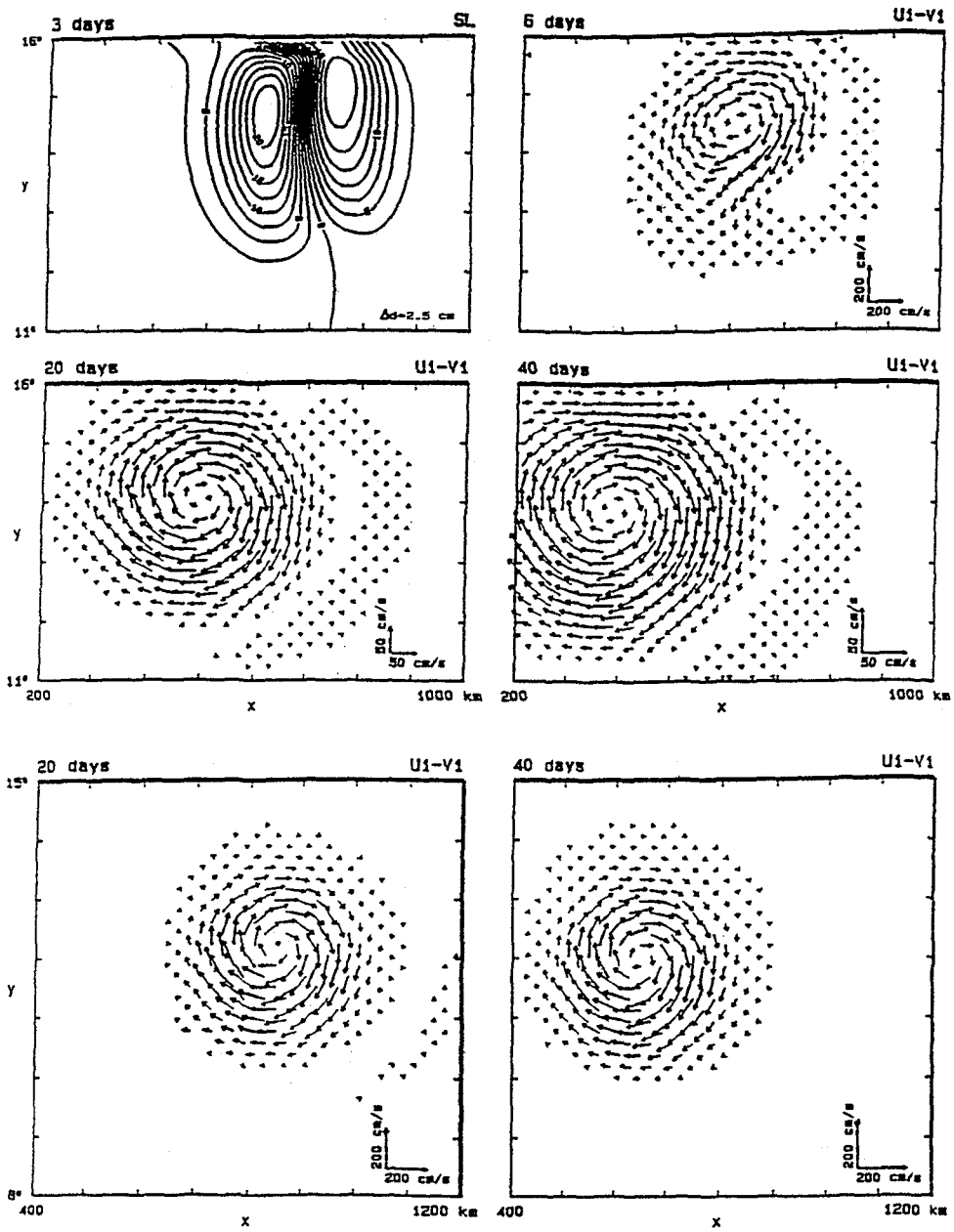

Fig. 4. The response of the nonlinear 1½-layer model with $T_a = 0°C$, showing sea level at day 3 and currents at day 6, 20 and 40 days to the Tehuantepec forcing (upper and middle panels), and currents at day 20 and 40 days to the Papagayo forcing (lower panels) for variable *f. The coastal sea-level drop was -23.0 cm which is less than -25.0 cm in Figure 11 in Lee(1990). The size of the Tehuantepec gyre is gradually growing due to larger mixing, and it propagates westward at a speed of 5.3 km/day. The Papagayo gyre does not grow rapidly with* $\upsilon_h = 2\times10^6$ cm^2/s at day 6, and its westward propagation speed is 10.3 km/day.

5-7 in McCreary *et al* (1989), except with $T_d = 0°C$ rather than 12°C. With this choice, the characteristic speed of the system, $c = [(g\varepsilon/\bar{\rho})(T_1 - T_d)H]^{½}$, increases to 206.5 cm/s, and so the Rossby radius and the non – dispersive Rossby wave speed are larger by factors of $(29/17)^{½} = 1.31$, and $29/17 = 1.71$.

respectively.

Generally, solutions for the two values of T_a are quite similar in structure. The upper two panels in Figure 4 show the initial response of the Tehuantepec solution, and they are comparable to two of the panels in their Figure 11 in McCreary *et al* (1989). The coastal sea-level drop at day 3 is actually less in Figure 4, being -23.0 cm rather than -25.0 cm. This property is somewhat surprising because the analytic solutions indicate that the drop increases with the parameter c; it happens because, according to (9), coastal sea level in the nonlinear model is influenced by the decrease in T as well as in h, and in this solution T drops only to 20.6°C (as compared to 14.4°C when T_a = 12°C). The middle and lower panels illustrate that the gyres propagate westward at speeds of 5.3 km/day and 10.3 km/day for the Tehuantepec and Papagayo solutions, respectively, faster because of the larger Rossby wave speed. These propagation speeds are in better agreement with the observations but still too small.

Solutions to the 2½-layer Model

a. Analytic solutions:

i. Uniform meridional wind, semi-infinite basin: To investigate how the existence of a second baroclinic mode affects the coastal sea-level drop, here we obtain analytic solutions to equations (1) without mixing on the *f*-plane forced by a spatially uniform, switched-on wind in a semi-infinite basin. Making the same assumptions that led to solution (19), the solution for the pressure field associated with each mode is given by

$$\tilde{p_n} = \frac{c_n \tau_0}{fH_n} e^{\alpha_n y} \mathcal{T}(t) \qquad (23)$$

Then, according to (7), the maximum coastal sea-level drop at day 3 is

$$d = \tilde{p}/g + \tilde{p_2}/g = \frac{c_1 \tau_o}{fgH_1} + \frac{c_2 \tau_o}{fgH_2}. \qquad (24)$$

For the parameters in Table 1, equation (24) shows that d= -(8.5 + 10.7) cm = -19.2 cm, which is 19% larger than the value of-16.1 cm from solution (19) for the 1½-layer model. So, coastal sea level is significantly affected by the presence of a second baroclinic mode in the inviscid, 2½-layer model.

ii. Wind periodic in x and t, semi-infinite basin, horizontal mixing: Here, we find analytic solutions to equations (1a) when there is mixing. The solution for each baroclinic mode is just (23) with c and H replaced with c_n and $\mathcal{H}_n$, respectively. Then, the maximum, coastal sea – level drop along the wind axis (at x = 0 and y = 0) at day 3 is $d = \tilde{d_1} + \tilde{d_2}$ = -17.8 cm, which is slightly larger than -16.8 cm of the 1½-layer model.
Therefore, the addition of a second baroclinic mode enhances the coastal sea-lavel drop when there is mixing, but only by 6%.

b. Numerical solutions:

i. Solutions in the Gulf of Tehuantepec: During the first 6 days the response of the no-nlinear 2½-layer model very similar to that of the nonlinear 1½-layer model. In addition, the sea-lavel drop at the coast increases to -26.2 cm, a 5% increase over the value of -25.0 cm for the nonlinear 1½-layer model. Figure 5 shows the Tehuantepec solution at 20 and 40 days for variable *f*, showing sea level, upper-and lower-layer currents, and temperature. SST patterns at 20 and 40 days are very similar to those in the nonlinear 1½-layer model, a relatively strong cyclonic gyre (speeds of the order of 14 cm/s at 20 days and 10 cm/s at 40 days) develops at the northeastern side of the anticyclonic one. The flow field in the second layer is also strong with the maximum speeds of about 18 cm/s at 20 days and 13 cm/s after 40 days. These upper and lower-layer flow fields both have a southward current that advects the anticyclonic gyre southward, and so the gyre locates at about 12.3°N after 40 days, much farther south than in the 1½-layer case. In one test run with $\upsilon_h = 2 \times 10^6$ cm^2/s after 6 days.

ii. Solutions in the Gulf of Papagayo: Figure 6 shows the response of the nonlinear 2½-layer

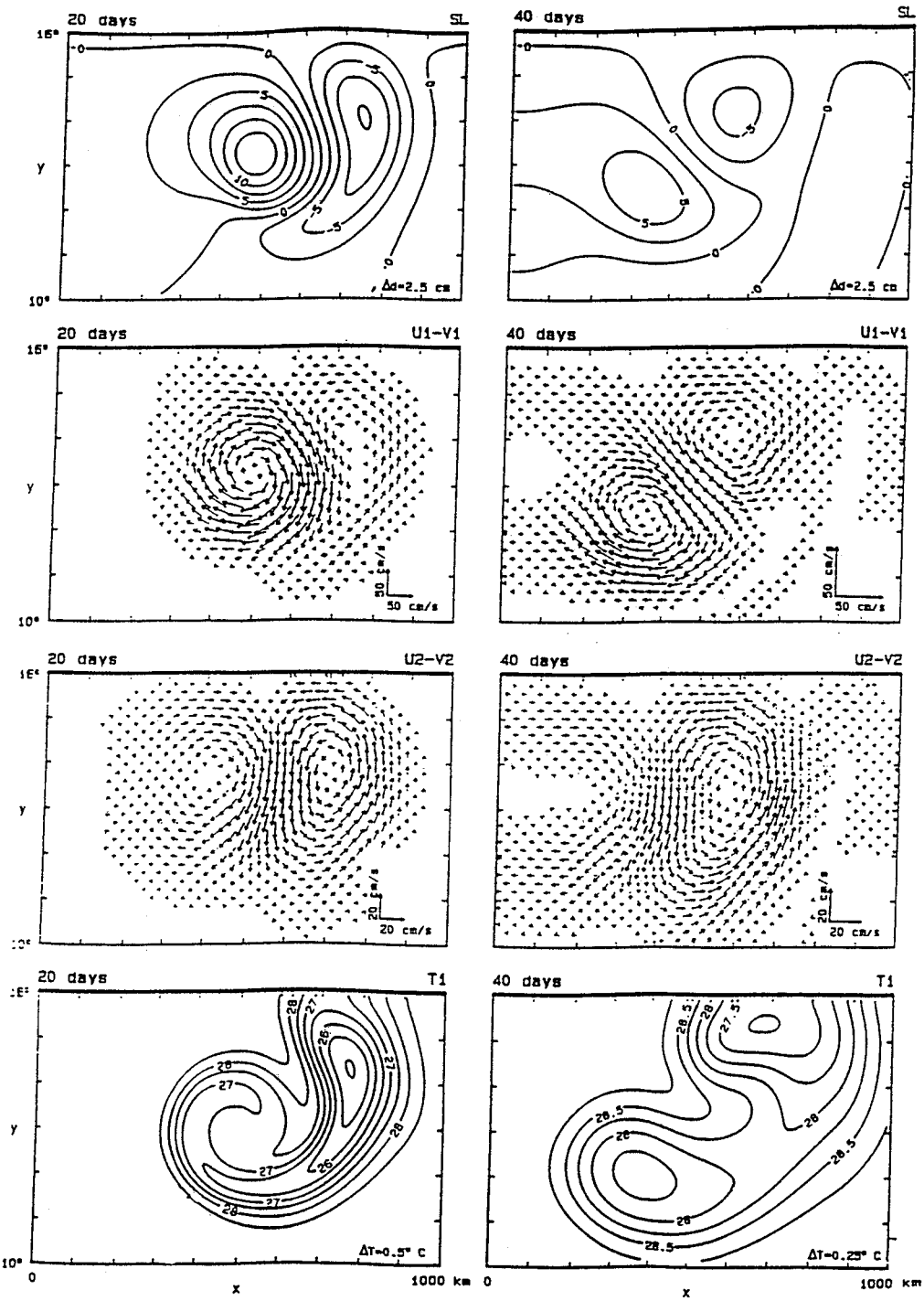

Fig. 5. The response of the nonlinear, 2½-layer model to the Tehuantepec forcing for variable f at 20 and 40 days, showing sea level, upper-layer and lower-layer currents,and temperature. The anticyclonic gyre propagates westward with a speed of about 6.0 km/day and also drifts southward due to self-advection and to advection by the lower-layer flow fields, and locates at 12.3 N after 40 days. A relatively strong upper-layer cyclonic circulation and by the southward lower-layer currents (18 cm/s at day 20 and 13 cm/s at 40).

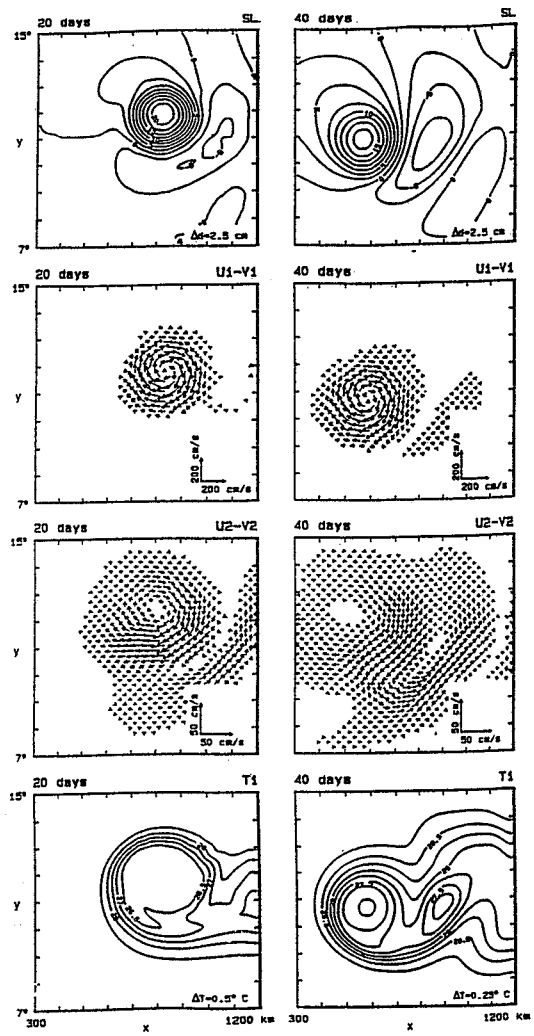

Fig. 6. The response of the nonlinear $2\frac{1}{2}$-layer model to the Papagayo forcing for variable f at 20 and 40 days. A relatively strong upper-layer cyclonic gyre (speeds of the order of 10 cm/s at 40 days) develops at the eastern flank of the anticyclonic gyre. Similarly, a southward lower layer currents (speed of the order of 30 cm/s at 20 days and 20 cm/s at 40 days) also pushes the anticyclonic gyre south-westward. The center of the gyre is at about 10.8 N at 40 days, and its propagation speed is about 12.8 km/day.

model to the Papagayo forcing at 20 and 40 days. At 20 days the response is almost same as that of the nonlinear $1\frac{1}{2}$-layer model. By day 40. however, the location of the gyre is shifted southward more than 1 degree farther. Its propagation speed increases with time from about 12 km/day to about 13 km/day, probably because f decreases as the gyre moves southward. Southward movement of the anticyclonic gyre in this case is due to the relatively strong second-layer flow field (20 cm/s) and to advection by the weak upper-layer cyclonic gyre. The average propagation speed from day 20 to 40 is about 12.8 km/day, which is very close to the observed speed of about 13 km/day. The increased westward propagation speed is largely due to advection by wind-forced background currents and partly due to the increased non-dispersive Rossby wave speed at lower latitudes.

To investigate how strongly the second – layer circulation affects the propagation speed of the gyre, we repeated the solution of Figure 6 with H_2 equaling 150 m and 450 m. With $H_2 = 150$ m, the resulting propagation speed of the gyre was about 14.5 km/day, and the strongest second-layer current speed was of the order of about 30 cm/s at day 40. With $H_2 = 450$ m, the resulting speed reduced to 10.5 km/day (similar to the $1\frac{1}{2}$-layer solution in the lower panels of Fig. 4) and the maximum speed of the second-layer current reduced to about 15 cm/s at day 40. Thus, the propagation speed appears to be directly related to the strength of the lower layer currents.

To investigate the influence of β and the effect of the second-layer flow field, we obtained and compared solutions to the nonlinear, $1\frac{1}{2}$-layer and $2\frac{1}{2}$-layer model with f constant. The nonlinear $1\frac{1}{2}$-layer anticyclone did not propagate westward at all. In this case, the anticyclone propagates westward with a speed of about 3.6 km/day, and this motion can only be due to the influence of the lower-layer circulation. Note that there are two nearly symmetric counter-rotating gyres in ths second layer with a maximum speed of about 30 cm/s. It is clearly westward advection induced by this dipole circulation pattern that accounts for the fast westward propagation speed of the upper-layer anticyclone. This result further supports the idea that the wind-forced Papagayo anticyclonic gyre propagates westward faster due to westward advection associated with background currents in the lower-layer.

SUMMARY AND DISCUSSION

This study investigates the coastal-ocean response to forcing by wind stress fields similar in structure to the narrow mountain-pass jets that occur in the Gulfs of Tehuantepec and Papagayo (Fig. 1). In response to this forcing, water moves rapidly offshore as the wind strengthens, and sea-level drops as much as 30 cm. The generation of an anticyclonic gyre that subsequently propagates westward and southward at a speeds considerably faster than that of a linear Rossby wave.

The model oceans used to study the dynamics of these phenomena are linear and non-linear versions of a 1½-layer model and a 2½-layer model, and most solutions are forced by idealized versions of the offshore jets (Fig. 2). The nonlinear models include an equation for the upper-layer temperature field with entrainment. Solutions are obtained both analytically and numerically. Solutions to the more sophisticated models compare remarkably well with the observations.

Analytic solutions to the linear 1½-layer model are found with f constant both with and without horizontal mixing. The solution with the northern boundary to the ocean [solution (19)]. In this case, there is a sea-level response at the coast that is directly proportional to the wind stress. The second is forced by a spatially confined wind field like the mountain-pass jets [solutions (20)]. It develops two symmetric gyres offshore due to Ekman pumping, has strong coastal currents that converge on the wind axis, and does not generate any coastal Kelvin waves. A third solution with horizontal mixing is found in a semi-infinite basin and forced by a wind that is uniform in y and periodic in x and $\mathcal{T}$ [solution (21)]. In this case, when $v_h = 2 \times 10^7 cm_{2/s}$ the coastal sea-level drop is enhanced to -16.8 cm and its phase is also shifted slightly in x and t, shifts do not occur in the inviscid analytic solutions. The reason for the increased sea-level drop is that the coastal boundary layer is actually narrower with horizontal mixing (right panel of Fig. 3), and so the interface must rise close to the surface in order to provide enough water for the volume that is moved offshore by the wind.

Numerical solutions to the linear 1½-layer model with f constant corroborate these an-alytic results, and demonstrate that horizontal mixing strengthens the coastal sea level response. Factors that increase the coastal sea-level drop during an upwelling event are: the offshore advection of thin h, and most importantly enhanced forcing τ/h in coastal regions where h is small. As for the linear model, horizontal mixing also strengthens the coastal sea level response by more than 30%. When f is variable, the gyres propagate westward with a speed less than that of nondispersive Rossby waves. The model Tehuantepec and Papagayo gyres propagate westward at speeds of 3.7 km/day and 6.3 km/day, faster than the speeds of linear Rossby waves, due partly to the increase of h at the center of the gyre and partly to self-advection. When T_a, the temperature of the deep ocean, is decreased from 12°C to 0°C, the speeds increase to 5.3 km/day and 10.3 km/day, respectively,largely due to the increase in the non-dispersive Rossby wave speed. existence of a second baroclinic mode increases the coastal sea-level drop. Solution (24) is forced by a spatially uniform, switched-on wind in a semi-infinite basin and has no horizontal mixing. The coastal sea-level drop in this case is -19.2 cm, 20% larger than the value of -16.1 cm for the corresponding solution (19) to the 1½-layer model. With horizontal mixing the solution forced by the same periodic wind as solution (24) has a maximum drop of -17.8 cm, an increase of 6% over the value of -16.8 cm for the 1½-layer model. Numerical solutions to the 2½-layer model also exhibit a most increased coastal sea-level drop, in one case a 5% increase from -25.0 cm for the nonlinear 1½-layer model to -26.2 cm for the 2½-layer model. In the Tehuantepec solution, the anticyclonic gyre moves southward due primarily to the strong lower-layer flow field. In the Papagayo solution, the lower-layer flow field advects the Papagayo gyre westward, increasing its westward propagation speed to 12.8 km/day (Fig. 6), Close to observed values. A solution with constant f corroborates how strongly the lower-layer currents modify the westward propagation speed; in the 1½-layer solution the gyre does not propagate westward at all, whereas in the 2½-layer solution it does at 3.6 km/day (not

shown here).

The propagation speeds of anticyclones are enhanced by advection in either of two ways: self-advection by β-induced distortions of the gyres themselves, and advection by background currents generated by the wind. To investigate the relative importance of these two processes, we found several solutions in which isolated eddies of approximately Gaussian shape were initially imposed on the models, and thereafter were left to develop freely. The $1\frac{1}{2}$-layer solutions has a westward propagation speed of 6.6 km/day, very close to that for the corresponding wind-forced gyre. In contrast, the isolated anticyclone in the $2\frac{1}{2}$-layer model propagates at a considerably slower speed than the wind-forced one does, indicating the importance of the wind-forced background circulation in the latter solution (not shown here).

In conclusion, the solutions presented here vary in complexity from a simple linear so-lution forced by a uniform wind in abounded ocean to complicated nonlinear solutions to a thermodynamic, $2\frac{1}{2}$-layer model that are forced by jet-like offshore directed winds. The resulting hierarchy of solutions reveals the important physics in an organized way.

Moreover, the solutions, particularly those of the nonlinear $2\frac{1}{2}$-layer model, compare remarkably well with the available observations, suggesting that they contain much of the important dynamics of the various phenomena. A logical next step in this area of research is to carry out calculations for a longer period with more realistic data.

ACKNOWLEDGMENTS

This research was supported by Korea Science and Engineering Foundation (921-0500-012-2). This work would not be published without the guidance and help of Julian P. McCreary and Kevin Kohler. Assistance of Soon Yong Kim was also great helpful.

REFERENCES

Alvarez, L.G., A. Barden-Dangon and A. Valle, 1989: On coastal currents off Tehuantepec. *Estuarine, Coastal and Shelf Science.*, **29**: 89-96.

Blackbun, M., 1962: An oceanographic study of the Gulf of Tehuantepec. U.S. Fish and Wildlife Service, Special Scientific Report-Fisheries No., 404, pp 28.

Clarke, A,J., 1988: Inertial wind path and sea surface temperature patterns near the Gulf of Tehuantepec and Gulf of Papagayo. *J. Geophys. Res.*, **93**: 15491-15501.

Crepon, M. and C. Richez, 1982: Transient upwelling generated by two-dimensional atmospheric forcing and variability in the castline. *J. Phys. Oceanogr.*, **12**: 1437-1457.

Enfield, D.B. and J.S. Allen, 1983: On the structure and dynamics of monthly mean sea level anomalies along the Pacific coast of North and South America. *J. Phys. Oceanogr.*, **10**: 557-578.

Haney, R.L., 1971: Surface thermal boundary conditions for ocean circulation models. *J. Phys. Oceanogr.*, **1**: 241-248.

Hua,B.L. and F.Thomasset, 1983: A numerical study of the effects of coastline geometry on wind-induced upwelling in the Gulf of Lions. *J. Phys. Oceanogr.*, **13**: 678-694.

Lee, Hyoung Sun, 1990: The coastal ocean response to strong offshore winds in the Gulfs of Tehuantepec and Papagayo. Ph d. Thesis.

Matsuura, T. and T.Yamagata, 1982: On the evolution of nonlinear planetary eddies layer than the radius of deformation. *J. Phys. Oceanogr.*, **12**: 440-456.

McCreary, J.P., Hyong S.Lee and D.B. Enfield, 1989: The response of the coastal ocean to strong offshore winds: With application to circulations in the Gulfs of Tehuantepec and Papagayo. *J. Mar. Res.*, **47**: 81-109.

McCreary, J.P. and P.K. Kundu, 1988: A numerical investigation of the Somali Current during the southwest monsoon. *J. Mar. Res.*, **46**: 25-58.

McWilliams, J.C. and G.R. Flierl, 1979: On the evolution of isolated nonlinear vorticies. *J. Phys. Oceanogr.*, **9**: 1155-1182.

Millot, C. and Crepon, M, 1981: Inertial oscillations on the continental shelf of the Gulf of Lions-Observations and Thoery, *J. Phys. Oceanogr.*, **11**: 639-656.

Nof,D., 1981: On the β-induced movement of isolated baroclinic eddies. *J. Phys. Oceanogr.*, **11**: 1662-1672.

Roden, G.I., 1961: On the wind-driven circulation in the Gulf of Tehuantepec and its effect upon surface temperatures. *Geofis. Int.*, **1**, 55-72.

Smith, D.C., IV and R.O. Reid, 1982: A numerical study of nonfrictional decay of mesoscale eddies. *J. Phys. Oceanogr.*, **12**: 244-255.

Stumpf, H.G., 1975: Satellite detection of upwelling in the Gulf of Tehuantepec, Mexico. *J. Phys. Oceanogr.*, **5**: 383-388.

Stumpf, H.G. and R. V. Legeckis, 1977: Satellite observations of mesoscale eddy dynamics in the eastern tropical Pacific Ocean. *J. Phys. Oceanogr.*, **7**: 648-658.

Trasvina, A., E.D. Barton, J.Brown, H.S. Velez, P.M. Kosro, and R.L. Smith, 1995: Offshore wind forcing in the Gulfs of Tehuantepec, Mexico: The asymmetric circulation. *J. Geophys. Res.*, **100**: 20649-20663.